Electronic Supplementary Material (ESI) for Nanoscale.

Mechanically Robust Nanocomposites from Screen-Printable Polymer/Graphene Nanosheet Pastes

Liqiang Zhang,[1,2] Rui Wang,[1] Jianlei Wang,[1] Lixin Wu,[1] and Xu Zhang*,[1]*

[1] CAS Key Laboratory of Design and Assembly of Functional Nanostructures, Fujian Provincial Key Laboratory of Nanomaterials, Fujian Institute of Research on the Structure of Matter, Chinese Academy of Sciences, Fuzhou, Fujian 350002, People's Republic of China

[2] College of Materials Science and Opto-Electronic Technology, University of Chinese Academy of Sciences, No.19 Yuquan Road, Shijingshan District, Beijing 100049, People's Republic of China

** Corresponding authors.*

E-mail address: lxwu@fjirsm.ac.cn (Lixin Wu), wyszhangxu@gmail.com (Xu Zhang)

Supporting Information

S1. XRD Analysis of PEI-rGO

XRD analysis was used to monitor the shift for GO. As shown in Figure S1, after surface modification by PEI, the XRD (002) peak of GO shifts from 9.4° to 24.44°, which clearly demonstrates the occurrence of reduction of GO.[S1]

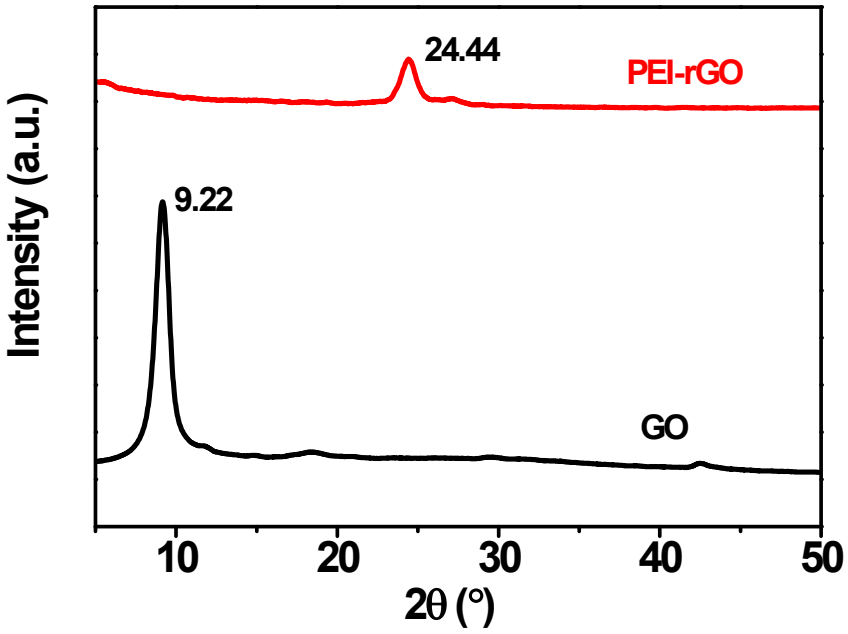

Figure S1. XRD spectroscopy of GO and PEI-rGO.

S2. FT-IR Analysis of PEI-rGO

Changes of the chemical composition in GO during the modification process were examined using FT-IR as shown in Figure S2. For pure GO, the characteristic peaks for -OH stretching band (3400 cm^{-1}), C=O stretching vibration (1720 cm^{-1}), C-OH (1350 cm^{-1}), and epoxy (1225 cm^{-1}) are consistent with the previously recorded data.[S2,S3] The spectrum of PEI-rGO indicates that C=O stretching vibration and epoxy disappears and the intensity of -OH stretching band was substantially decreased, most likely owing to the reduction by PEI. In addition to this, two new characteristic peaks, primary amine group (C-NH, 1524 cm^{-1}) and secondly amine group (HNC=O, 1647 cm^{-1}) stretching vibrations, were observed, which might come from amidation reaction and nucleophilic substitution reaction between the amine group of PEI and the epoxy and carboxyl group on GO.[S1,S4]

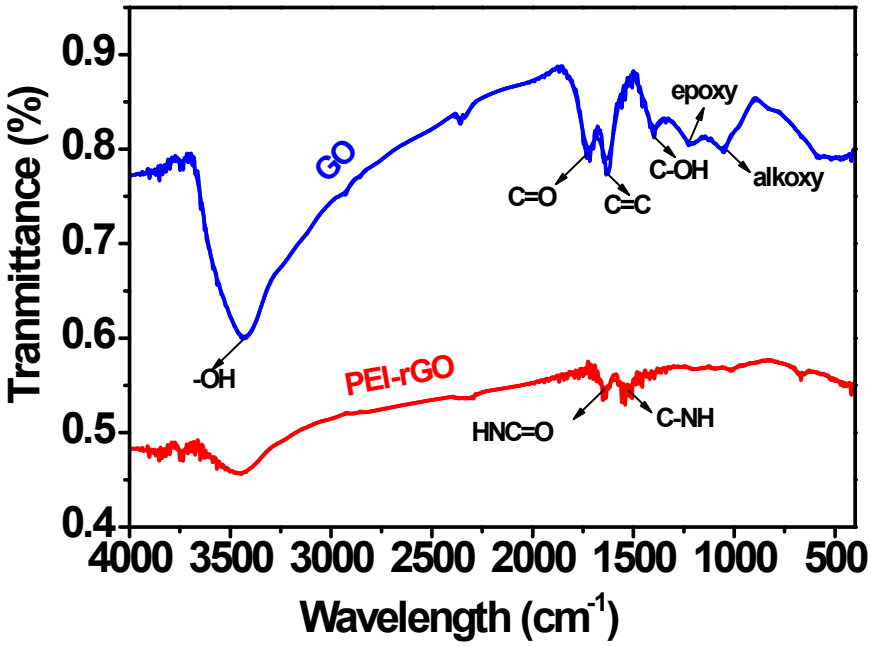

Figure S2. FT-IR spectra of GO and PEI-rGO.

S3. Screen Printer

printer setup used in our experiments shown in Figure S3 mainly consists of frame and stencil. The thickness of stencil is important setup parameter for paste printing. In general, a thinner stencil is conducive to effective screen printing because it more easily allows the paste to flow through the stencil and transfer onto the substrate, but it should be more than 75 μm in order to tolerate the applied force during printing.[S5] The stencil used here is at a thickness of 105 ± 5 μm so that it is flexible yet strong enough to be fit for screen printing.

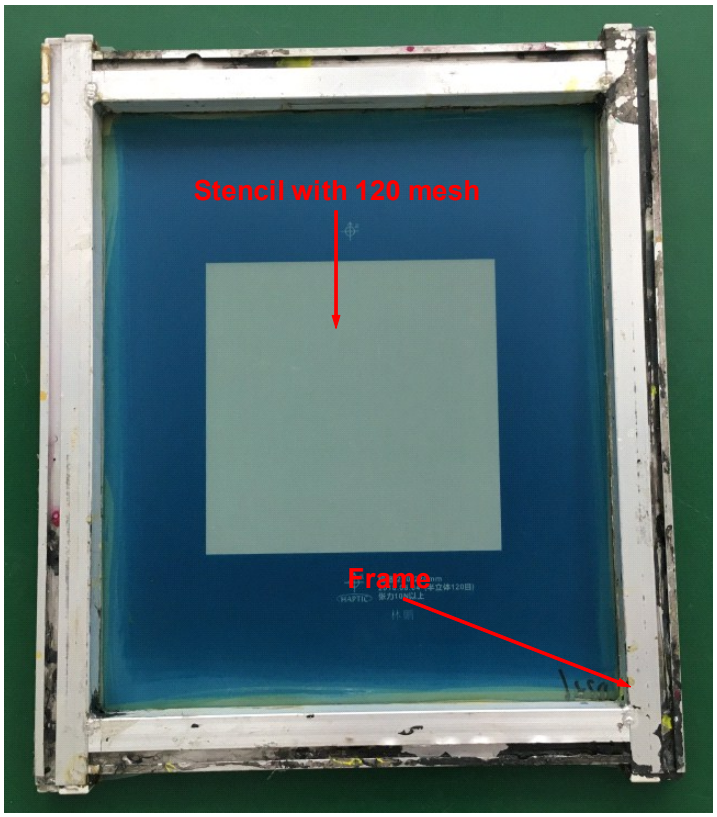

Figure S3. The picture of screen printer

S4. Screen Printing Process from Cross Section View

Step 1: The formulated WPU/PEI-rGO paste was first loaded over nylon stencil.

Step 2: A squeegee is then drawn across it, forcing the paste through the open pores and making it contact with glass substrate simultaneously.

Step 3: The penetrated paste adheres to substrate and conglutinate together because of its excellent shapeability and thixotropic characteristic.

Step 4: The squeegee was removed from stencil, which separated from substrate at the same time and leaved the paste on the printing area to form nanocomposites by water evaporation process followed.

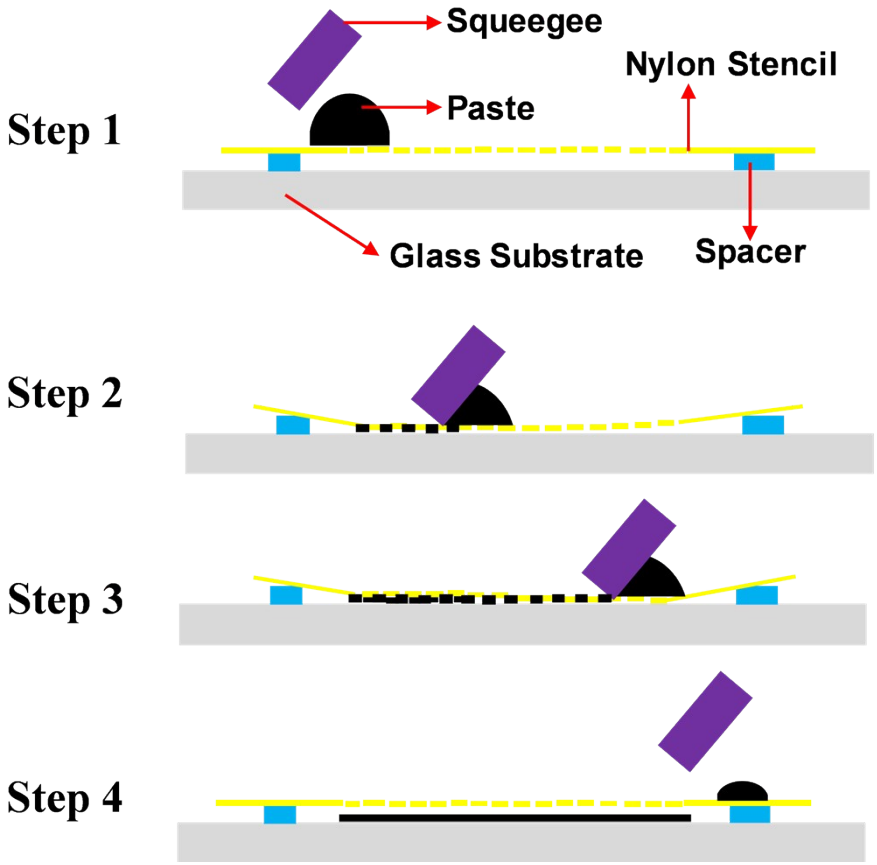

Figure S4. Schematic diagram of screen printing from a cross section view.

S5. Details of Mechanical Properties

Table S1. Mechanical properties of WPU, WPU/GO, and WPU/PEI-rGO nanocomposites.

Sample	Tensile Strength (MPa)	Increment (%)	Young's Modulus (MPa)	Increment (%)
WPU	1.50 ± 0.3		1.05 ± 0.2	
WPU/PEI-rGO-0.2	3.61 ± 0.5	140.2	2.09 ± 0.4	99.1
WPU/GO-0.5	5.76 ± 0.6	288.4	4.56 ± 0.7	334.3
WPU/PEI-rGO-0.5	9.01 ± 1.1	500.9	8.63 ± 0.9	721.9
WPU/GO-0.8	10.55 ± 0.8	603.7	12.62 ± 1.2	1157.1
WPU/PEI-rGO-0.8	14.06 ± 1.2	837.8	15.35 ± 0.8	1362.1
WPU/PEI-rGO-1.0	15.27 ± 0.9	946.6	21.84 ± 1.4	1979.9

S6. Justification of Halpin-Tsai Models

In the main manuscript, we introduced classical Halpin-Tsai models to predict the Young's modulus of nanocomposites. In order to more logical to get these values, we justified the models because the graphene is a typical 2D sheet rather than effective fiber filler. The modified models based on the geometry and orientation of reinforcement filler were recorded with the following equations.[S6-S8]

$$E_{\text{c-random}} = E_{\text{PM}}\left(\frac{3}{8}\cdot\frac{1+\xi\eta_{\text{L}}V_{\text{FG}}}{1-\eta_{\text{L}}V_{\text{FG}}}+\frac{5}{8}\cdot\frac{1+2\eta_{\text{W}}V_{\text{FG}}}{1-\eta_{\text{W}}V_{\text{FG}}}\right) \quad (1)$$

$$E_{\text{c-parallel}} = E_{\text{PM}}\times\frac{1+\xi\eta_{\text{L}}V_{\text{FG}}}{1-\eta_{\text{L}}V_{\text{FG}}} \quad (2)$$

$$\eta_{\text{L}} = \frac{E_{\text{G}}/E_{\text{PM}}-1}{E_{\text{G}}/E_{\text{PM}}+\xi} \quad (3)$$

$$\eta_{\text{W}} = \frac{E_{\text{G}}/E_{\text{PM}}-1}{E_{\text{G}}/E_{\text{PM}}+2} \quad (4)$$

$$\xi = \frac{\text{W}+\text{L}}{t} \quad (5)$$

$$V_{\text{FG}} = \frac{\text{W}_{\text{FG}}}{\text{W}_{\text{FG}}+(\rho_{\text{FG}}/\rho_{\text{PM}})(1-\text{W}_{\text{FG}})} \quad (6)$$

Where $E_{\text{c-random}}$ and $E_{\text{c-parallel}}$ is Young's modulus of the nanocomposites films with randomly and parallelly oriented graphene nanosheets, respectively. The E_{PM} and E_{G} stands for the Young's modulus of WPU and graphene, respectively. The L, W, and V_{FG} represents the average length, width, and volume fraction of the functionalized graphene (PEI-rGO), respectively. The thickness and average length of PEI-rGO are measured to be about 1.13 nm and 3.2 μm from the atomic force microscope (AFM) analysis. The density of pure WPU and PEI-rGO is around 1.19 g/cm^3 and 1.85 g/cm^3, respectively. The Young's modulus of pure WPU is tested to be 1.5 MPa from at least 5 nanocomposites sample tests. The Young's modulus of PEI-rGO is approximately 300 GPa derived from the previously convincing study,[S9,S10] namely $E_{\text{G}} \approx E_{\text{FG}}$. The calibrated parameter ξ in equation (5) is mainly related to the geometry and boundary condition of reinforced filler based on Halpin-Thomas models for rectangular filaments. The equation (6) is used to convert weight fraction to

volume fraction for calculating the Young's modulus. The V_{FG}, W_{FG}, and ρ_{FG} is volume, weight, and density fraction of PEI-rGO, respectively. The ρ_{PM} is the density of polymeric matrix. By substituting equations (3), (4), (5), and (6) into (1) and (2), the final calculated equations can be expressed by equations, (7) and (8):

$$E_{\text{c-random}} = \frac{3}{8}E_{\text{PM}} \times \frac{1+V_{\text{FG}}\left[(\text{W}+\text{L})/t\right]\left[\dfrac{E_{\text{FG}}/E_{\text{PM}}-1}{E_{\text{FG}}/E_{\text{PM}}+(\text{W}+\text{L})/t}\right]}{1-V_{\text{FG}}\left[\dfrac{E_{\text{FG}}/E_{\text{PM}}-1}{E_{\text{FG}}/E_{\text{PM}}+(\text{W}+\text{L})/t}\right]} + \frac{5}{8}E_{\text{PM}} \times \frac{1+2V_{\text{FG}}\left[\dfrac{E_{\text{FG}}/E_{\text{PM}}-1}{E_{\text{FG}}/E_{\text{PM}}+2}\right]}{1-V_{\text{FG}}\left[\dfrac{E_{\text{FG}}/E_{\text{PM}}-1}{E_{\text{FG}}/E_{\text{PM}}+2}\right]} \tag{7}$$

$$E_{\text{c-parallel}} = E_{\text{PM}} \times \frac{1+V_{\text{FG}}\left[(\text{W}+\text{L})/t\right]\left[\dfrac{E_{\text{FG}}/E_{\text{PM}}-1}{E_{\text{FG}}/E_{\text{PM}}+(\text{W}+\text{L})/t}\right]}{1-V_{\text{FG}}\left[\dfrac{E_{\text{FG}}/E_{\text{PM}}-1}{E_{\text{FG}}/E_{\text{PM}}+(\text{W}+\text{L})/t}\right]} \tag{8}$$

S7. Thermogravimetric Analysis

Table S2. The decomposition temperature of WPU, WPU/GO, and WPU/PEI-rGO nanocomposites. The $T_{5\%}$ and $T_{50\%}$ stand for temperature at 5% and 50% weight loss, respectively.

Samples	$T_{5\%}$ (°C)	$T_{50\%}$ (°C)
WPU	189	377.2
WPU/PEI-rGO-0.2	195	380.6
WPU/GO-0.5	202	383.5
WPU/PEI-rGO-0.5	209	388.4
WPU/GO-0.8	215	390.2
WPU/PEI-rGO-0.8	224	391.5
WPU/PEI-rGO-1.0	234	393.6

S8. Bonding Strength Analysis

The bonding properties between the paste and the textile is indeed a fundamental consideration. The bonding strength is strongly affected or even decided by the nature of polymer matrix coated on textile.[S11,S12] The WPU used here is a sort of polymer targeted for textile surface treatment or adhesive applications and the bonding is strong enough to meet the industrial standard (Footwear Industrial Test Standard: G80-W/B Adhesive Compatibility; the generic specification is that the minimum value of bonding strength is expected to be over 27 N/cm for textiles and synthetic leathers). To see the effect of modified graphene on bonding strength of nanocomposites from pastes, the adhesive strength measurement was performed based on the industrial standard mentioned above and the testing details can be seen in *Adhesive Compatibility Test* and Figure S5 below. The data give the information that incorporating graphene filler into WPU has very little effect on bonding properties since very low level (below 1.0 wt%) was incorporated to WPU, but importantly which adequately meets the requirements of industrial applications (over 27 N/cm). The bonding strength of pure WPU and nanocomposites ranges from 37.8 + 2.5 N/cm (nanocomposites containing 1.0wt% modified graphene) to 41.3 + 1.8 N/cm (pure WPU), figures for the other specimens were in between.

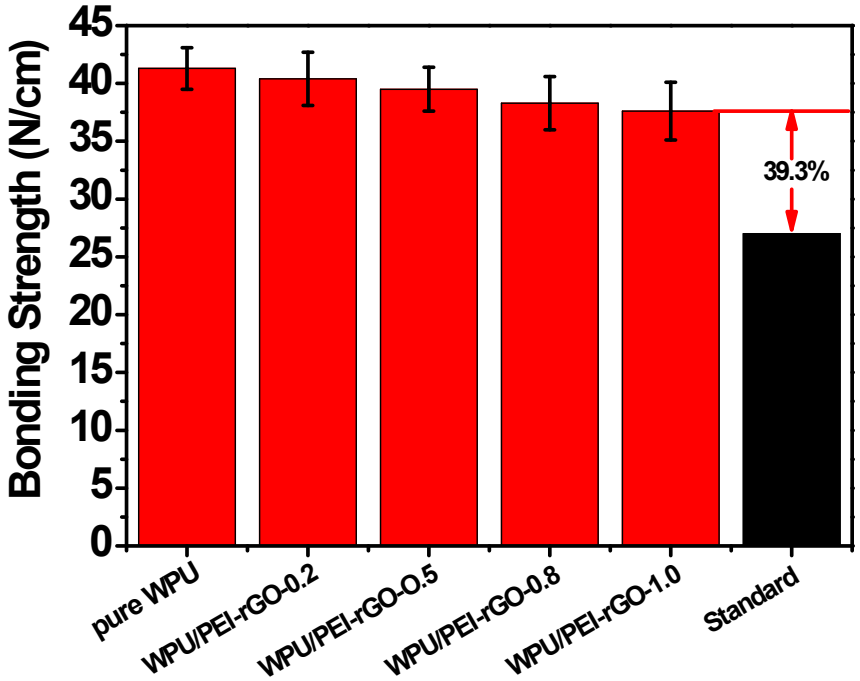

Figure S5. Bonding strength of the WPU, WPU nanocomposites and standard.

Adhesive Compatibility Test

1. Specimen preparation based on standard: ISO 2418.

Firstly, the textile printed with formulated pastes was cut into rectangular samples (approximately 1 cm × 15 cm). Secondly, adhesive joint design of T-peel strength measurement: two identical samples (side of textile printed with paste) were tightly bonded by water-based cement (The one used here is super-strong cement: NO 906N. Bonding strength for textile is well over 100 N/cm). The two sides of the sample in the one end must remain separated for purpose of mounting the specimen in the T-peel tester and starting the test. The final step for specimen preparation is to mark off 2.5 cm from the end of each sample that was not laminated. This will be the area to pull apart to start the test and then mark five additional 2.0 cm section as shown in Figure S6 below.

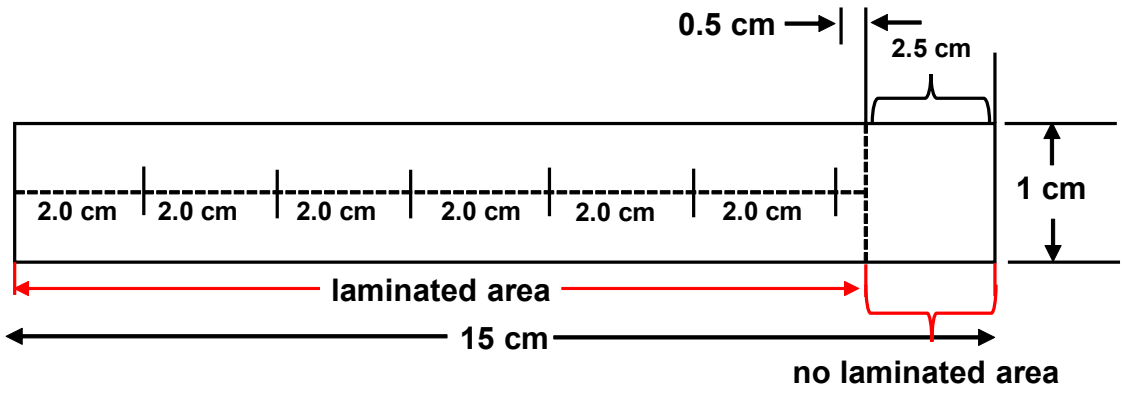

Figure S6. Schematic diagram of specimen for adhesive compatibility test.

2. T-peel strength measurement[S13]

The first step is to carefully separate about 0.5 cm of two components (upper nanocomposites form pastes and textile) by machine. The samples were then clamped straight between two grips before pulling using Servo Control Universal Testing Machine (AG-8000 S, Dongguan Aogoan Instrument Co. Ltd., P. R. China). The final stage is to start the test at the speed of 50 mm min^{-1} and to record the data of bonding strength (Figure S5), when there was a clear and distinct bond separation between

the two material in testing process, which demonstrate that bond strength between paste and textile is more than 39.3% than that of standard requirement.

Note: If an area of bond failure is seen between marks, record the bond failure value. The exact bond failure is an average value from five marked areas and each bond strength came from three samples.

S9. Abrasion Resistance Test

Abrasion tests were carried out following ASTM D-3884, employing a Taber abrasion machine (Figure S7a). The Taber machine equipped with two loaded abrasive wheels (250 g in total), against which the nanocomposites sample is rubbed using a rotational platform. The testing sample includes a carboard backer with adhesive and thickness 0.8 ± 0.2mm, which is tightly bonded with the testing sample having the same diameter. A 6 mm diameter hole was drilled in the center of the well-cohesive testing sample to help secure it on the rotational platform of the Taber machine (Figure S7b). Based on the ASTM standard, one rotation of the assisted support (carboard backer) was counted as one cycle. All tests were conducted under the normal room temperature (23 ± 2 ℃, with a humidity of 50% ± 5%). The abrasive particles or small fragments coming on the surface of sample during abrasion process could be easily absorbed by dust collector. The mechanical durability performance is measured by mass loss tested periodically and plotted in Figure 10a.

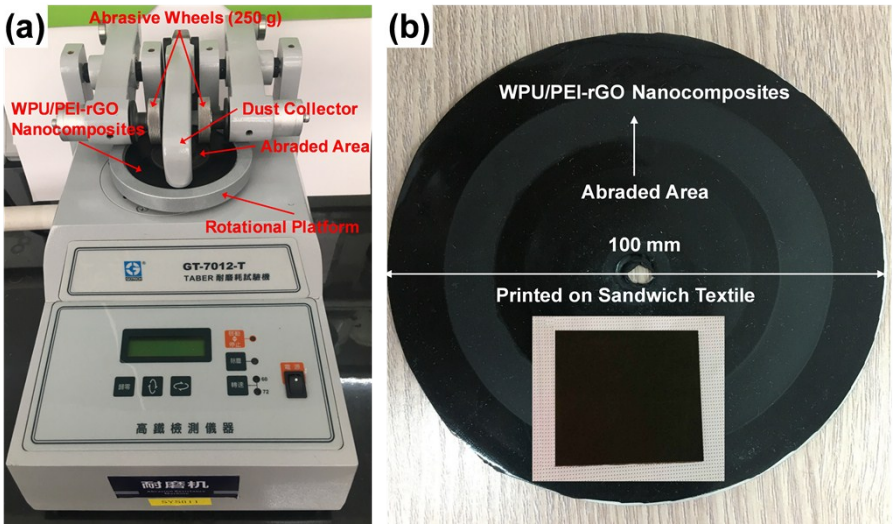

Figure S7. (a) The picture of Taber Abrasion machine featuring abrasive wheels, dust collector and rotational platform. (b) A WPU/PEI-rGO nanocomposites sample bonded with 0.8 mm carboard backer with central hole for mounting on the Taber machine.

References

(S1). S. Roy, X. Z. Tang, T. Das, L. Y. Zhang, Y. M. Li, S. Ting, X. Hu and C. Y. Yue, *ACS Appl. Mater. Interfaces*, 2015, **7**, 3142-3151.

(S2). D. A. Dikin, S. Stankovich, E. J. Zimney, R. D. Piner, G. H. B. Dommett, G. Evmenenko, S. T. Nguyen and R. S. Ruoff, *Nature*, 2007, **448**, 457-460.

(S3). D. Li, M. B. Müller, S. Gilje, R. B. Kaner and G. G. Wallace, *Nat. Nanotechnol.*, 2008, **3**, 101-105.

(S4). G. Yu and P. Wu, *Polym. Chem.*, 2014, **5**, 96-104.

(S5). D. A. Pardo, G. E. Jabbour and N. Peyghambarian, *Adv. Mater.*, 2000, **12**, 1249-1252.

(S6). J. C. H. Affdl and J. L. Kardos, *Polym. Eng. Sci.*, 1976, **16**, 344-352.

(S7). X. M. Feng, W. Y. Xing, H. Y. Yang, B. H. Yuan, L. Song, Y. Hu and K. M. Liew, *ACS Appl. Mater. Interfaces*, 2015, **7**, 13164-13173.

(S8). R. Gunawidjaja, C. Jiang, S. Peleshanko, M. Ornatska, S. Singamaneni and V. Tsukruk, *Adv. Funct. Mater.*, 2006, **16**, 2024-2034.

(S9). C. Lee, X. Wei, J. W. Kysar and J. Hone, *Science*, 2008, **321**, 385-388.

(S10). P. Poulin, R. Jalili, W. Neri, F. Nallet, T. Divoux, A. Colin, S. H. Aboutalebi, G. Wallace and C. Zakri, *Proc. Natl. Acad. Sci. U. S. A.*, 2016, **113**, 11088-11093.

(S11). M.SSánchez-Adsuar, *Int. J. Adhes. Adhes.*, 2000, **20**, 291-298.

(S12). G. de Avila Bockorny, N. L. Preuss, C. R. I. Gomes, N. S. D. Junior, M. M. de Camargo Forte, *Matéria (Rio J.)*, 2018, 23(4), DOI: 10.1590/s1517-707620180004.0581.

(S13). M. A. Pérez-Limiñana, F. Arán-Aís, A. M. Torró-Palau, A. C. Orgilés-Barceló and J. M. Martín-Martínez. *Int. J. Adhes. Adhes.*, 2005, **25**, 507-517.